Observation of magnetic state dependent thermoelectricity in superconducting spin valves

César González-Ruano[†],[1] Diego Caso[†],[1] Jabir Ali Ouassou,[2] Coriolan Tiusan,[3, 4] Yuan Lu,[4] Jacob Linder,[2] and Farkhad G. Aliev[5, *]

[1]*Departamento Física de la Materia Condensada C-III,*
Universidad Autónoma de Madrid, Madrid 28049, Spain
[2]*Center for Quantum Spintronics, Department of Physics,*
Norwegian University of Science and Technology, NO-M7T9Q Trondheim, Norway
[3]*Department of Solid State Physics and Advanced Technologies,*
Faculty of Physics, Babes-Bolyai University, Cluj Napoca 400114, Romania
[4]*Institut Jean Lamour, Nancy Universitè, 54506 Vandoeuvre-les-Nancy Cedex, France*
[5]*Departamento Física de la Materia Condensada C-III,*
Instituto Nicolás Cabrera (INC) and Condensed Matter Physics Institute (IFIMAC),
Universidad Autónoma de Madrid, Madrid 28049, Spain

Superconductor-ferromagnet tunnel junctions demonstrate giant thermoelectric effects which are being exploited to engineer ultra-sensitive terahertz radiation detectors. Here, we experimentally observe the recently predicted complete magnetic control over thermoelectric effects in a superconducting spin valve, including the dependence of its sign on the magnetic state of the spin valve. The description of the experimental results is improved by the introduction of an interfacial domain wall in the spin filter layer interfacing the superconductor. Surprisingly, the application of high in-plane magnetic fields induces a double sign inversion of the thermoelectric effect, which exhibits large values even at applied fields twice the superconducting critical field.

INTRODUCTION

The competition between superconducting (S) and ferromagnetic (F) ground states can under certain conditions result in a synergy of these otherwise antagonistic states [1]. In recent years, a variety of exotic phenomena have been demonstrated in devices that exploit this synergy. Notable examples include long-ranged spin-triplet supercurrents [2–4], spin-valve Josephson junctions [5], superconducting spin-valves with record-high magnetoresistance, and the giant thermoelectric (TE) effect. These effects are considered as potential ingredients in the next generation of low-dissipation cryogenic devices [6–8].

In general, there exists considerable interest in identifying material platforms for improved TE devices. At low temperatures, TE effects are expected to be vanishingly small in both normal metals and bulk superconductors. Instead, they have been investigated mainly in superconductor/normal-metal hybrids, where they have been used in micro-refrigeration and thermometry [9]. More recently, fascinating theoretical predictions [10–15] have opened the door to unexplored spin dependent TE effects in S/F hybrids. The transport of spin and charge due to temperature gradients in such systems have only been investigated experimentally in a few works [16–19]. Kolenda *et al.* [16] reported on the experimental observation of an enhanced Seebeck coefficient (up to $100\,\mu V/K$) when a large magnetic field of about 1 T splits the quasiparticle band structure of a superconductor. When combined with a spin-filtering magnetic interface, this spin splitting breaks the electron–hole symmetry of the junction. The resulting carrier asymmetry produces the observed "giant TE effect", which is now being exploited to develop ultrasensitive radiation detectors [20].

So far, the experimental tuning of giant TE effects in S/F hybrids has been carried out either by applying large magnetic fields [16] or by exchange coupling a superconductor to a ferromagnetic insulator [20]. Recently, however, a different method to control the TE effect has been predicted in superconductor/ferromagnet/ferromagnetic insulator systems [21]. This method can turn the superconducting TE effect on and off *in situ*, as well as reversing its sign. Here, by interfacing a superconductor with a spin valve with large spin filtering capability, we experimentally demonstrate the above mentioned complete magnetic control of the superconducting TE effect. This includes evidence of an antisymmetric TE effect, where a change of the magnetic state of the spin valve inverts the direction of the TE current. Controlling the sign of the thermopower, analogous to the inversion of TE signals between *p*- and *n*-doped semiconductors, enables the design of Peltier elements based on superconducting spin valves.

EXPERIMENTAL RESULTS

Figure 1(a) illustrates the main experimental set-up and junctions investigated. We have measured TE effects in V(40)/MgO(2)/Fe(10)/MgO(2)/Fe(10)/Co(30) single crystalline junctions epitaxially grown on MgO(001) substrates, with the thickness of each layer given in nanometers in parentheses. More details about the junctions, experimental set-up and procedures can be found in the Supplemental Material sections 1 and 2. Here, V is a BCS superconductor, Fe and Co are ferromagnetic metals, and MgO is a symmetry filtering insulator. The magnetically hard Fe/Co electrode allows for a precise detection of the orientation of the magnetically free Fe layer interfacing the superconductor. Figure 1(b)-(c) presents a general electron transport characterization of the junctions in the superconducting state as a function of the applied bias and external magnetic field. One observes that the superconducting gap in the V electrode is suppressed by in-plane (IP) and out-of-plane (OOP) fields of about 1.7 T and 0.4 T, respectively (Fig. Figure 1(c)). As we will discuss fur-
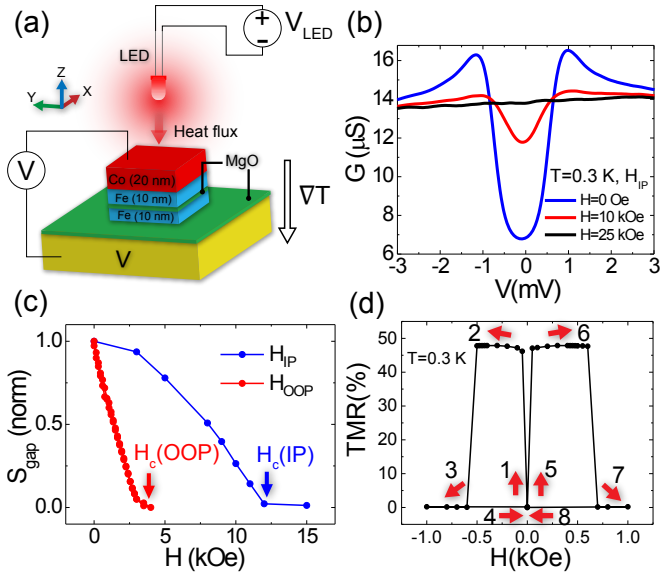
FIG. 1: (a) Sketch of the S/F/F junctions when heated by a LED. (b) Typical conductance–bias curves measured at $0.07T_c$ at three different applied IP magnetic fields. (c) Normalized superconducting gap depth (S_{gap}) taken from $G(V)$ curves vs applied IP and OOP magnetic fields. (d) Typical tunneling magnetoresistance curves measured with IP magnetic field at $V = 5$ mV and $T = 0.3$ K. The numbers indicate the order of the field sweeping and resistance changes.
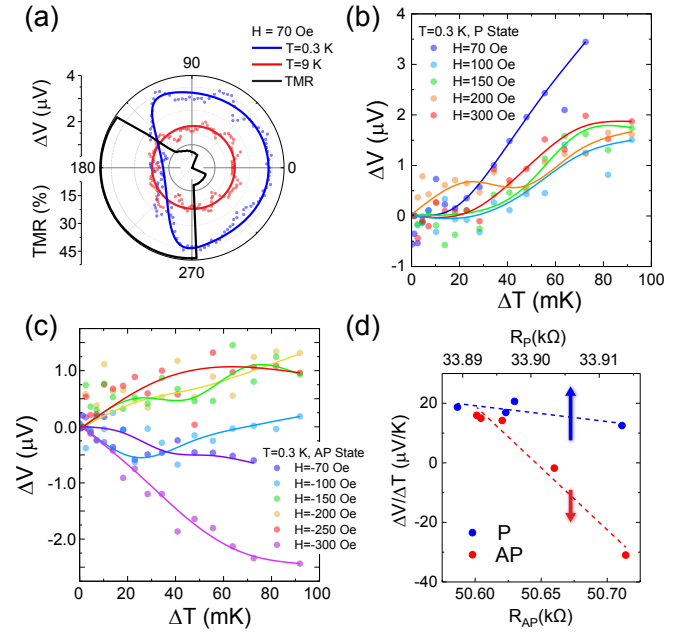

FIG. 2: Thermoelectric response of a S/F/F junction measured under a rotation and fixed values of the applied magnetic field at $T = 0.3$ K. (a) TE response at $H = 70$ Oe for in-plane rotations of the magnetic field at $V_{LED} = 7.3$ V ($\Delta T \approx 113$ mK), below and above T_c. The tunnel magnetoresistance of the spin-valve is also displayed against the rotation angle. (b) Response in the P configuration of the spin-valve stack. (c) Same experiment for the AP configuration. The TE voltage changes its sign and intensity depending not directly on the applied field, but on the saturation of the soft FM layer. The related analysis is shown in panel (d), where the average value of the TE voltage is plotted against the measured resistance for the P (blue, upper horizontal axis) and AP (red, lower horizontal axis) configurations. For the P state, a lower resistance implies a better polarization, while in the AP state the polarization is better with a higher resistance.

ther below, the magnetoresistance values of 35-55% provide an estimation of the effective spin polarization of the Fe electrodes of around 0.75–0.85 for the different junctions studied based on the Julliere model, involving two ferromagnetic and one nonmagnetic (V) electrodes, in line with previous reports [22].

To study the TE effect as a function of the spin-valve state, the soft Fe layer was rotated while the hard Fe/Co layer remained fixed. We did this by applying a rotating in-plane magnetic field, with a magnitude between the coercive fields of the two magnetic layers. For the hard layer the coercive field is typically larger than 500 Oe (Fig. 1(d)), while for the soft layer it's smaller than 50 Oe, determined by the magneto-crystalline anisotropy. This procedure guarantees a reorientation between the parallel (P), antiparallel (AP) and perpendicular in-plane (PIP) configurations of the spin valve. For each 3° rotation of the applied field, the temperature gradient ∇T was re-established via the LED heater, and the resulting TE response ΔV was measured.

Fig. 2(a) shows the variation of the TE voltage generated during a magnetization rotation of the free layer under an in-plane applied magnetic field of 70 Oe. While the transition between the P and PIP states hardly affects the values of the TE response, a strong reduction of the TE voltage of more than a factor of 2 is observed when the free layer becomes close to AP to the fixed Fe/Co layer. Note that there is a slight latency of about 10–15° between the angle of the applied magnetic field and the real average magnetization orientation of the

Fe layer. This is a natural consequence of the experimental process: the Fe magnetization has to overcome the magneto-crystalline anisotropy to follow the slowly rotating applied field (see for example Ref. [23]). The complete 360° rotation takes about two hours, since we stop at each intermediate angle to measure the TE response. Figures Fig. 2(b) and (c) show the TE response of the samples vs the induced temperature gradient for different magnetic configurations and applied fields. Note that these temperature gradients have been estimated by first simulating the response to the incoming heat flux and subsequently recalculating ΔT from V_{LED} based on the LED calibration curves (see Supplemental Material sections 4 and 5). In the P state, changing the applied field by less than a few hundred Oe does not qualitatively change the TE response (Fig. 2(b)). However, in the AP state, varying the magnetic field has a dramatic effect on the TE response and can even change its sign as seen in Fig. 2(c). We note that no asymmetry of ΔV or dependence on V_{LED} was observed above T_c (Fig. 2(a)). Control experiments on short-circuited junctions also revealed at least an order of magnitude drop of the TE response regardless of
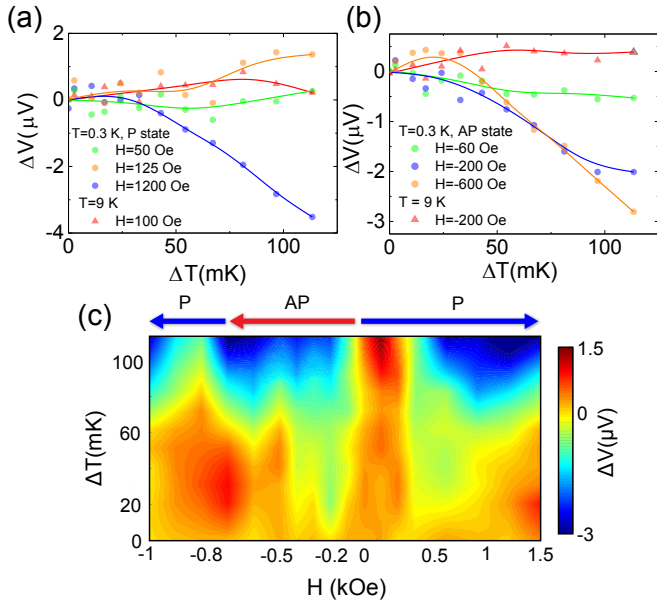
FIG. 4: (a) Thermoelectric voltage of an S/F/F and S/F junction at $V_{\mathrm{LED}} = 7.3$ V ($\Delta T \approx 113$ mK) vs. applied in-plane field at $T = 0.3$ K. The high-field sign inversion is achieved in both samples, and the TE effect is maintained with increasing in-plane fields up to 30 kOe. The inset displays the measured TE voltage in the S/F/F junction under out-of-plane field. At $H = H_c$, superconductivity and its associated TE voltage vanish. (b) TE inversion field and polarization against the maximum TMR value for all the S/F/F junctions under study.

FIG. 3: Thermoelectric voltage of an S/F/F junction demonstrating sign inversion at high fields in the P state (a) and AP state (b). (c) Colormap of the recorded TE voltage ΔV as a function of the temperature difference ΔT and the applied in-plane field H for the same junction, indicating the P and AP states.

the magnetic state (see Supplemental Material section 6).

In order to understand the possible reasons for the TE sign change in the AP state, we analyzed (Fig. 2(d)) the TE response obtained for a fixed temperature gradient as a function of the resistance in the P and AP states obtained during each particular TE experiment at different applied in-plane magnetic fields (not exceeding 500 Oe). While the TE response in the P state is rather robust to the variation of the resistance (i.e. presence of magnetic inhomogeneities), in the AP state it changes sign with the *reduction* of the influence of these magnetic textures (an increase of the resistance means better magnetization saturation).

Interestingly, some junctions revealed a TE sign inversion both in the AP state and also under a sufficiently high applied in-plane magnetic field in the P state (Fig. 3). The TE response in the P state is positive and robust at fields below 0.5 kOe (Fig. 3(a)), and becomes negative for higher magnetic fields. In contrast, in the AP state the TE response is already negative for much smaller fields (Fig. 3(b)), right after the spin-valve switched into the AP state (see steps 1-2 in Fig. 1(d)). Further increasing the negative magnetic field (path 2-3 in Fig. 1(d)) reorients the hard layer so the spin-valve is again in the P configuration, and again the sign of the TE effect follows the same trend as for positive fields. Figure 3(c) summarizes these observations with a 3D color plot of the TE voltage signal against the applied field and evaluated temperature gradient.

We have found that the TE voltage sign inversion in the P state under high in-plane magnetic fields is a rather robust effect and is followed by a second TE sign inversion towards
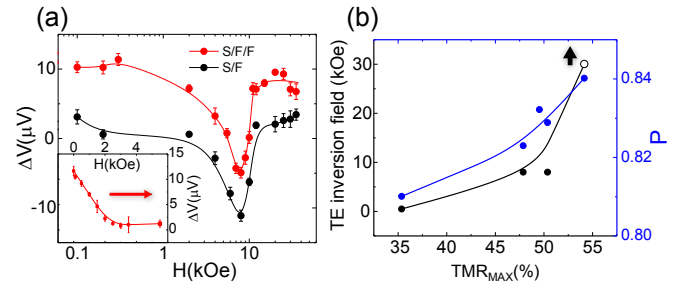
positive values when the magnetic field is further increased (Fig. 4(a)). Surprisingly, even for maximum applied in-plane magnetic fields, twice exceeding the second critical magnetic field (compare Fig. 1(c) and Fig. 4(a)), the TE voltage remains high and without clear signatures of diminishing. A qualitatively similar response has been observed in single barrier V/MgO/Fe junctions, i.e. without the sensing Fe/Co layer. Fig. 4(b) compares the TE signal inversion field with the TMR and effective spin polarization values of each corresponding sample. Apparently, a higher TMR and correspondingly polarization values shift the TE inversion field range outside our experimental capabilities (35 kOe). This suggests a possible link between the observed effect and interfacial domain wall forming in the Fe electrode. Further experiments are needed to understand the physical mechanism behind the high field TE effects.

THEORETICAL MODELLING

To better understand the physics behind the experimental observations, we explored the setup in Fig. 1(a) via numerical simulations. We employed the Usadel formalism [24–28] which describes superconductivity in diffusive heterostructures, together with spin-dependent tunneling boundary conditions [10, 29–32] valid for arbitrary spin polarizations. To numerically solve these equations, we used the Ricatti parametrization [33, 34] to calculate spectral properties and a distribution-trace parametrization [26–28, 35] to calculate the nonequilibrium transport properties. The theoretical and numerical approach is described in more detail in Ref. [21].

The numerical model used herein is sketched in Fig. 5(a). The superconductor (V) was treated as a BCS superconducting reservoir with an effective spin-splitting $h = \Delta/10$, near-zero temperature $T = T_c/100$, and electrical grounding $V = 0$. The hard ferromagnet (Fe/Co) was treated as a non-superconducting metallic reservoir at an elevated temperature $T = T_c/2$ and volt-

age $V = \Delta V$. The interfaces to the soft ferromagnet (V/MgO/Fe and Fe/MgO/Fe/Co) were treated using spin-polarized tunneling boundary conditions with spin polarizations P_1, P_2 and a low tunneling conductance $G_T = G_D/5$ where G_D is the Drude conductance of the soft ferromagnet. These parameters model the high spin filtering capabilities and low transparencies of the MgO barriers. In the soft ferromagnet (Fe), we used an exchange splitting $h = 30\Delta$. For each magnetic configuration, we (i) solved the Usadel equation for 80 different $e\Delta V/\Delta \in [-0.04, +0.04]$; (ii) used this to calculate the current $I(\Delta V)$; (iii) interpolated the open-circuit voltage from $I(\Delta V) \equiv 0$. This yielded the TE voltage as function of magnetic configuration.

The magnetic configurations we considered are illustrated in Fig. 5(a–b). We take the hard ferromagnet (red) to be oriented along one in-plane axis (up), and the spin filtering at the MgO barrier is assumed to be parallel to this orientation (black). The soft ferromagnet is then rotated by an in-plane angle φ relative to the hard ferromagnet (purple), which here is sketched for the antiparallel case $\varphi = \pi$. At the superconductor interface, we include the possibility for an interfacial domain wall described by an out-of-plane angle θ. This affects both the spin filtering at the second MgO barrier (black) and the direction of spin splitting inside the neighboring superconductor (blue). Fig. 5(c–e) show the numerical results for the TE voltage $\Delta V(\varphi)$ across the junction as function of the in-plane misalignment angle between the two ferromagnets. In panel (c), we see the predicted response for a junction with two identical spin filters ($P_1 = P_2$) and no interfacial domain wall ($\theta = 0$). We then predict an *asymmetric TE effect*, by which we mean that $\Delta V(0)$ is maximal while $\Delta V(\pi) \to 0$. This can intuitively be understood as follows. If the two spin filters are identical ($P_1 = P_2$ and $\varphi = 0$), then "filtering the spins twice" does not significantly change the physics compared to having only one spin filter. The latter case has in previous work been shown to produce a giant TE effect in superconductor/ferromagnet systems [10–19]. On the other hand, the effects of two identical but oppositely aligned spin filters cancel, so any TE effect due to spin filtering should vanish for $\varphi = \pi$. In panel (d), we see the case of different spin filters ($P_1 < P_2$). It is now possible for one ferromagnet to dominate the spin splitting of the superconducting density of states, while the other dominates the spin filtering process. Via the mechanism explored in detail in [21], this leads to an antisymmetric contribution to $\Delta V(\varphi)$, whereby $\Delta V(0)$ and $\Delta V(\pi)$ have opposite signs. In the extreme case of $P_1 \ll P_2$ the result is a purely antisymmetric shape for $\Delta V(\varphi)$, whereas for P_1, P_2 of similar magnitude the theory predicts $|\Delta V(\pi)| \ll |\Delta V(0)|$. In panel (e), we show the effect of adding an out-of-plane interfacial domain wall to panel (d), which clearly suppresses the antisymmetric contribution.

While the simplest model presented in Fig. 5(c) captures the essential features of Fig. 2(a), including an interfacial domain wall in the model enhances the agreement with the experiment. Specifically, in the absence of externally applied fields, such a domain wall would produce the results in panel Fig. 5(e), which also agrees well with Fig. 2(a). However, as the in-
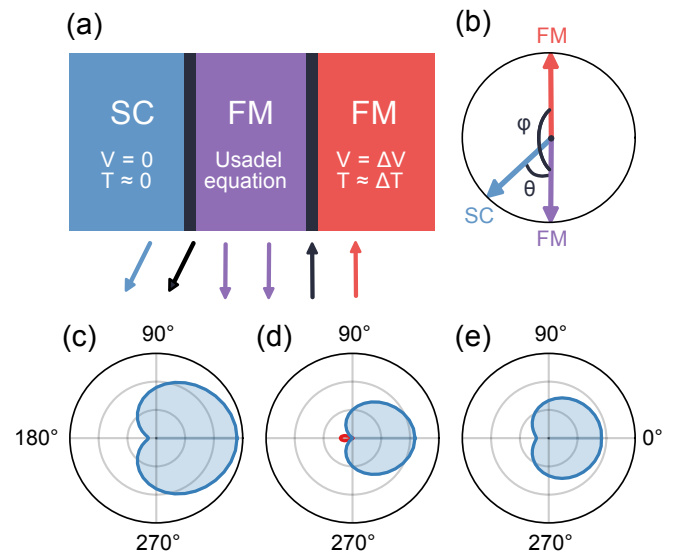

FIG. 5: (a) Numerical model, including field directions (shown here for the AP configuration). (b) Definitions of angles θ and φ with respect to the field directions in the model. (c–e) Numerical results for the magnetically dependent thermoelectric voltage $\Delta V(\varphi)$. Blue and red correspond to positive and negative voltages, while the radius in each plot is $|\Delta V| = 0.04\Delta/e$ where e is the elementary charge. The three plots correspond to (c) $\theta = 0$, $P_1 = P_2 = 80\%$; (d) $\theta = 0$, $P_1 = 60\%$, $P_2 = 80\%$; (e) $\theta = \pi/4$, $P_1 = 60\%$, $P_2 = 80\%$.

plane applied field is ramped up, the domain wall should be rotated into the thin-film plane: $\theta \to 0$. In this case, we would gradually move towards panel (d), where $\Delta V(\varphi)$ changes sign. This qualitatively agrees with the experimental observations in Fig. 2d, where it is found that $\Delta V(\pi)$ changes sign for increasing magnetic saturation while $\Delta V(0)$ changes only slightly.

DISCUSSION AND CONCLUSIONS

While our numerical modelling qualitatively explains the experiments at low magnetic fields where the switching between the P and AP states takes place (Figs. 2, 3 and 5), it does not account for the unexpected strong variation of the TE response in the high field limit, where a double sign change takes place regardless of the presence of the magnetically hard layer (Fig. 4). This is because the spin-resolved particle-hole asymmetry in quasiclassical theory is only present in the superconducting state. A possible factor which may influence the high field TE response is a transformation of the interfacial magnetism at the V/MgO interface [36] under an applied magnetic field. Initially predicted by numerical simulations [37], spin fluctuations and/or surface atomic layer magnetism in V have been under debate for decades now [38–42]. In our experiments, a sufficiently large in-plane magnetic field could transform the V/MgO interface into an additional, atomically-thin magnetic layer. The induced surface magnetism might strongly affect the exchange splitting of the electron bands in V.

The explanation of the high-field TE response behavior remains an intriguing open problem.

In conclusion, we report on the experimental control of the superconducting thermoelectric effect using a spin-valve device with a spin filter. We demonstrate both experimentally and by numerical simulations the transition from a strongly asymmetric to an anti-symmetric response depending on the saturation of the AP alignment of the spin-valve, which is likely modulated by an interfacial domain wall. Furthermore, our results point towards an unexpected thermoelectric response in superconductor/ferromagnet junctions under high in-plane magnetic fields. More detailed experimental and theoretical studies are required to understand this behaviour.

†C.G.-R and D.C. contributed equally to the manuscript.

SUPPLEMENTAL MATERIAL

1. Samples and experimental set-up

The superconductor–spin-valve multilayer stacks have been grown by molecular beam epitaxy (MBE) in a chamber with a base pressure of 5×10^{-11} mbar while the crystalline quality was controlled by in-situ RHEED measurements, following the procedure described in Ref. [43]. The resulting layered structures were then lithographed into squared samples with lateral sizes ranging from 30×30 to 60×60 μm^2.

The measurements are performed inside a JANIS He^3 cryostat (minimum attainable temperature is 0.3 K). The magnetic field is varied using a 3D vector magnet consisting of one solenoid (X axis) with $H_{\max} = 3.5$ T and two Helmholtz coils (Y and Z axis) with $H_{\max} = 1$ T.

2. Experimental procedures for the TE response measurements

In order to produce a temperature gradient in the samples, a commercial Light Emitting Diode (LED) was placed above the sample (see Fig.1 of the main text). Voltage was supplied to the LED (model LUXEON 3030 2D) by a Keithley 228A voltage source. The LED started to emit light at an applied bias of 5.6 V at room temperature. As no direct visual contact could be established inside the cryostat, the thermometer and voltage source were used to check the LED functioning at low temperatures: First, the thermometer closer to the samples showed a steady increase in temperature when the applied voltage was above 6 V. Second, the compliance indicator present in the Keithley voltage source showed the same signal at this voltage than it did at room temperature when the LED was on.

Once this was established, the TE voltage (ΔV) is measured as follows: first, the resistance and temperature of the sample are measured, and then voltage measurements are taken with an applied current of $I = 0$ nA (using the smallest available current range in the Keithley 220 current source, which has a maximum compliance current of $I = 1.9995$ nA and a minimum step of 500 fA with an accuracy of ±2 pA). Then, the LED is turned on with the desired voltage (V_{LED}), and a second voltage measurement is taken at zero current after 2 seconds, before the LED is turned off again. We checked that the voltage readings were stable for waiting times between 1 and 10 seconds after turning on the LED. We chose the 2 seconds because it ensures the gradient temperature without overheating the sample during the experiments. Each voltage measurement is taken using the smallest measuring range of the DMM-552 voltmeter card, and averaging over 100 voltage readings.

We have carried out three types of thermoelectric measurement experiments. First, the magnetic field rotations that have been explained in the experimental results section. Secondly, the TE response of the spin-valve (S/F/F) samples was studied separately in each magnetic configuration. This was done by setting the desired magnetic orientation (i.e. parallel (P) or antiparallel (AP) state) at a fixed temperature (usually below T_c at $T = 0.3$ K or above T_c at 9 K) and field magnitude, and measuring the TE voltage ΔV for increasing values of the LED heater voltage V_{LED}. The sample was let to cool down for a minute after each heating experimental point in order to avoid overheating. The whole process was repeated 5 to 10 times and averaged for each V_{LED} to reduce the uncertainty. This was made for different magnetic orientations of the sample, as shown in Figs. 2 and 3 on the main text, where instead of V_{LED}, the corresponding estimated temperature difference ΔT between the Fe and V electrodes is shown (see details on the temperature gradient evaluation below).

The third type of experiments study the TE response as a function of the applied magnetic field direction for fixed values
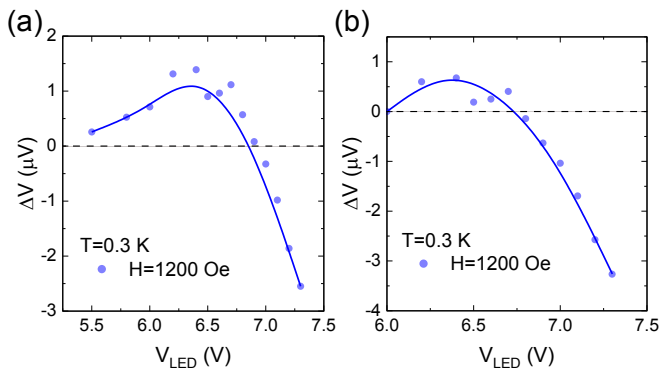
FIG. 6: (a) TE voltage observed in a S/F/F junction vs LED voltage at $T = 0.3$ K ($H = 1200$ Oe). The voltage background level has not been removed yet. (b) Same TE voltage vs V_{LED} curve as in panel (a) after the background voltage subtraction.
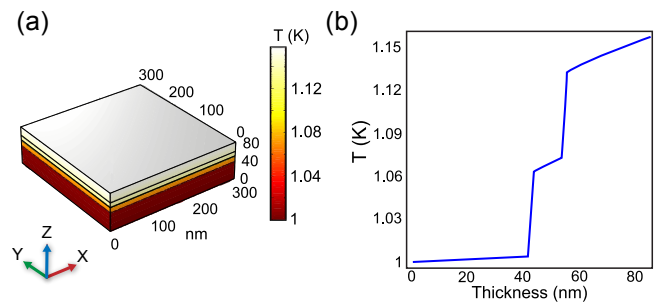

FIG. 7: COMSOL modelling of the S/F/F system. (a) 3D model of the junction temperature distribution, with a net heat flux of 6.7×10^{-6} W entering from the top. (b) Temperature profile along the Z direction.

of V_{LED}. In all of the experiments, the low bias resistance (at about 5 mV) was also measured, allowing for a precise detection of the magnetization configuration of the free Fe layer. More details on the electric transport measurements, along with the samples characterization, can be found in Ref. [44]

3. Background voltage removal

Some of the plotted TE voltage curves such as Figs. 2(b–c), 3(a–c) and 4(a) on the main text were constructed assuming negligible ΔT up until $V_{LED} = 6$ V, considering that below this voltage practically no temperature gradient was induced between the superconductor and ferromagnet (see Fig. 8(d) inset). Figure 6(a) shows a typical TE voltage curve against the LED voltage, from 5.5 to 7.3 V. As TE effects seen at voltages below $V_{LED} = 6$ V are not related with the heat produced by the LED, we assume that they are a consequence of the unavoidable background temperature gradient in the S/F/F junction due to the thermalization process with the cryostat cooling system (He^3 pot). Accordingly, the background voltage was removed on all of the mentioned plots. Fig. 6 displays an example of background TE signal removal for one of the curves.

4. MODELLING OF THE TEMPERATURE PROFILE

The thermal response of the system was modelled using COMSOL [45]. The following section explains the modelling for a fixed voltage of the LED heater of 7 V as a representative example, since this was one of the most used voltage values where the TE response was evaluated.

The LED heater worked at 7 V with an applied current of 0.3 mA. The total dissipated power in this situation is therefore 2.1 mW. The heater is located at a distance of ~ 1 cm from the sample, so the power per unit area reaching the surface of the sample holder is estimated as 6.7 W/m². The measured

samples surface varies from 30×30 to 60×60 μm² depending on the sample, but the structure is grown as a pillar and located under a gold contact with a surface of approx 1×1 mm². We will first assume that all of the energy that falls onto the pillar is transmitted into the sample's top layer. Therefore the total heat flux entering the sample is taken as 6.7×10^{-6} W. The total temperature gradient had an approximately linear dependence with this total flux and therefore applied voltage of the LED heater.

The thermal conductivity and heat capacity of each of the materials (Co, Fe, MgO and V) at low temperatures was taken from tabulated values in the literature [46–49]. The model in COMSOL assumes that the bottom of the V layer has a fixed temperature of 1 K and the lateral faces are isolated (since the sample is in a vacuum chamber in the cryostat). With these parameters, the temperature difference between the Fe and V layers is in the range of 70 mK (see Fig. 7). With the observed TE voltage in the order of ~ 3 μV, this would make for a Seebeck coefficient of ~ 50 μV/K, which is in the same order of magnitude of previous similar studies [50].

5. RESCALING V_{LED} INTO ΔT

Once the temperature gradient was estimated for a fixed bias of $V = 7$ V with the COMSOL simulations, the whole ΔV vs. V_{LED} curves that were measured for the different studied samples had to be recalibrated into ΔV vs. ΔT. For this, first we took a look at the technical datasheet of the LED used in the experiments, from which luminosity vs current (fig. 8(a)) and current vs. voltage (Fig. 8(b)) curves were obtained. By composing these two curves we obtained a luminosity vs voltage curve our LED. As the curves were obtained at room temperature, the applied voltage axis had to be re-scaled in order to fit the behavior of the LED at low temperatures: for the minimum working voltage, we looked at the temperature values measured by the thermometer during V_{LED} sweeps, observing that the LED started heating the sample at an applied bias of ~ 6 V (vs 5.6 V at room T). As for the maximum luminosity bias value, we observe that the Keithley 228A power supply
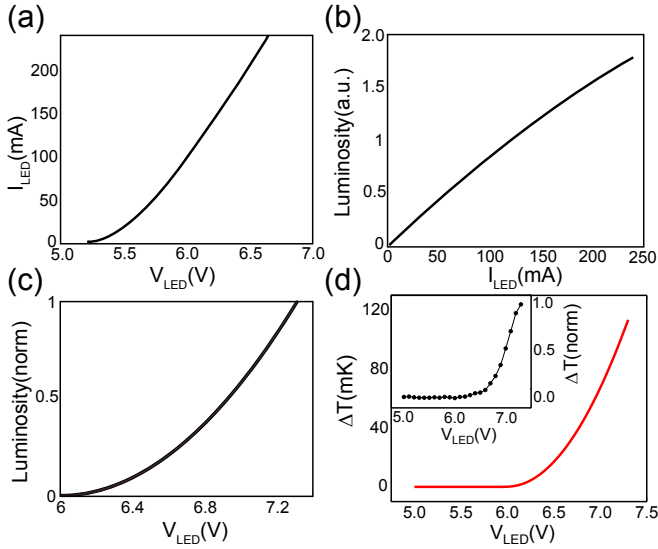
FIG. 8: (a) Intensity vs applied bias curve at room temperature for the commercial LED that was used during the experiments (model LUXEON 3030 2D). (b) Luminosity vs current curve, for the same LED. (c) Normalized luminosity vs applied voltage curve, constructed by composing the two previous ones and with the voltage range already rescaled to the LED behavior at low temperatures. (d) ΔT vs V_{LED} constructed from the curve in (c) plus the COMSOL simulation results. The inset shows the normalized increase in temperature measured experimentally with the thermometer closest to the sample inside the cryostat during a V_{LED} sweep. Note that this does not correspond to the temperature gradient ΔT established in the junction, as it is only a local measure near the samples. Nevertheless, the two curves qualitatively match, which is a good indicator for the reasonable validity of the estimated ΔT gradient under the LED heating.

FIG. 9: Thermoelectric response of a short-circuited S/F/F sample. (a) Thermoelectric voltage for 200 Oe and −200 Oe at $T = 0.3$ K. (b) 3D representation of the TE voltage against the in-plane field and ΔT at $T = 0.3$ K.

any value of the LED heating and magnetic field. The results suggest that the electric-channel was short-circuited, which was accompanied by a strongly enhanced thermal conductivity and therefore a reduced temperature gradient.

could not exceed 7.35 V during normal operation when the LED was connected. With this, we can re-scale the luminosity vs V_{LED} curve (Fig. 8(c)). The last step is to assume that the heating will be directly proportional (i.e. linear dependence) to the emitted luminosity of the LED, and use 2 points to calibrate the slope: the base point of $V_{LED} = 6$ V at which ΔT is assumed to be zero, and the simulated point of $V_{LED} = 7$ V for which an estimation of $\Delta T = 150$ mK was obtained with COMSOL. Putting all together, we finally have the ΔT vs. V_{LED} curve (Fig. 8(d)), which was used to transform the ΔV vs. V_{LED} experiments into the presented ΔV vs ΔT graphs.

6. THERMOELECTRIC RESPONSE IN A SHORT-CIRCUITED S/F/F JUNCTION

We carried out control experiments of the TE response in short-circuited junctions. By operating at relatively high applied biases (between 1 and 2 V), a pinhole was induced in the MgO barriers of one of the samples where the TE response was being studied. The outcome was a close to 10^3 drop in the resistance, from kOhms to tens of Ohms. The result is shown in Fig. 9, revealing an absence of TE generated voltage for
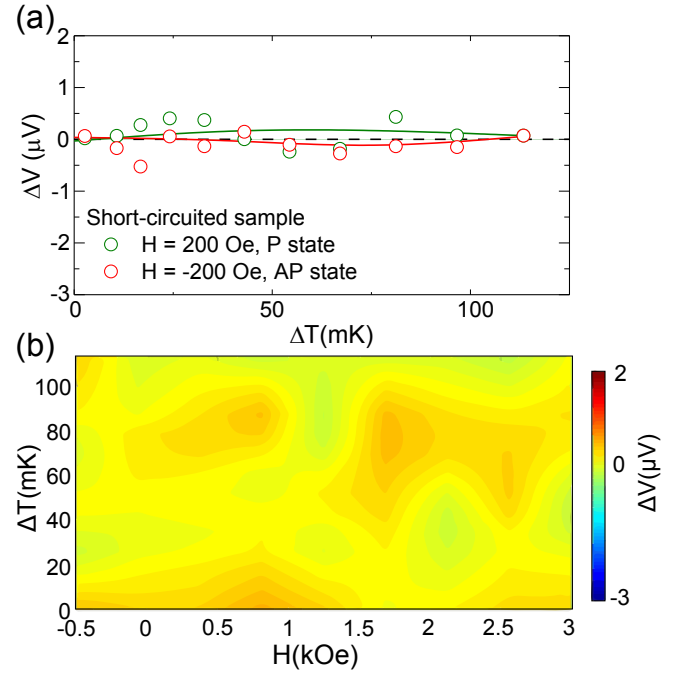
* e-mail: farkhad.aliev@uam.es

[1] A. I. Buzdin, Proximity effects in superconductor-ferromagnet heterostructures, Rev. Mod. Phys. 77, 935 (2005).

[2] R. S. Keizer, S. T. B. Goennenwein, T. M. Klapwijk, G. Miao, G. Xiao, and A. Gupta, A spin triplet supercurrent through the half-metallic ferromagnet CrO_2, Nature 439, 825 (2006).

[3] J. W. A. Robinson, J. D. S. Witt, M. G. Blamire, Controlled Injection of Spin-Triplet Supercurrents into a Strong Ferromagnet, Science 329, 59 (2010)

[4] Trupti S. Khaire, Mazin A. Khasawneh, W. P. Pratt, Jr., and Norman O. Birge, Observation of Spin-Triplet Superconductivity in Co-Based Josephson Junctions, Phys. Rev. Lett. 104, 137002 (2010).

[5] B. M. Niedzielski, T. J. Bertus, J. A. Glick, R. Loloee, W. P. Pratt, Jr. and N. O. Birge, Spin-valve Josephson junctions for cryogenic memory, Phys. Rev. B 97, 024517 (2018).

[6] G. Yang, C. Ciccarelli, and J. W. A. Robinson, Boosting spintronics with superconductivity, APL Materials 9, 050703 (2021).

[7] A. E. Madden, J. C. Willard, R. Loloee, and N. O. Birge, Phase controllable Josephson junctions for cryogenic memory, Supercond. Sci. Technol. 32, 015001 (2018).

[8] L. Ai, E. Zhang et al. Van der Waals ferromagnetic Josephson

junctions, Nat Commun **12**, 6580 (2021).

[9] F. Giazotto, T. T. Heikkilä, A. Luukanen, A. M. Savin and J. P. Pekola, Opportunities for mesoscopics in thermometry and refrigeration: Physics and applications, Rev. Mod. Phys. **78**, 217 (2009).

[10] P. Machon, M. Eschrig, and W. Belzig, Nonlocal Thermoelectric Effects and Nonlocal Onsager relations in a Three-Terminal Proximity-Coupled Superconductor-Ferromagnet Device, Phys. Rev. Lett. **110**, 047002 (2013).

[11] P. Machon, M. Eschrig, and W. Belzig, Giant thermoelectric effects in a proximity-coupled superconductor–ferromagnet device, New J. Phys. **16** 073002 (2014).

[12] A. Ozaeta, P. Virtanen, F. S. Bergeret, and T. T. Heikkila, Predicted very large thermoelectric effect in ferromagnet-superconductor junctions in the presence of a spin-splitting magnetic field, Phys. Rev. Lett. **112**, 057001 (2014).

[13] M. S. Kalenkov and A. D. Zaikin, Electron-hole imbalance and large thermoelectric effect in superconducting hybrids with spin-active interfaces, Phys. Rev. B **90**, 134502 (2014).

[14] P. Dutta, A. Saha and A. M. Jayannavar, Thermoelectric properties of a ferromagnet-superconductor hybrid junction: Role of interfacial Rashba spin-orbit interaction, Phys. Rev. B **96**, 115404 (2017).

[15] T. Savander, S. Tamura, C. Flindt, Y. Tanaka and P. Burset, Thermoelectric detection of Andreev states in unconventional superconductors, Phys. Rev. Research **2**, 043388 (2020).

[16] S. Kolenda, M. J. Wolf and D. Beckmann, Observation of Thermoelectric Currents in High-Field Superconductor-Ferromagnet Tunnel Junctions, Phys. Rev. Lett. **116**, 097001 (2016).

[17] S. Kolenda, P. Machon, D. Beckmann and W. Belzig, Nonlinear thermoelectric effects in high-field superconductor-ferromagnet tunnel junctions, J. Nanotechnol. **7**, 1579–1585 (2016).

[18] S. Kolenda, C. Surgers, G. Fischer, and D. Beckmann, Thermoelectric effects in superconductor-ferromagnet tunnel junctions on europium sulfide, Phys. Rev. B **95**, 224505 (2017).

[19] J. Heidrich and D. Beckmann, Nonlocal thermoelectric effects in high-field superconductor-ferromagnet hybrid structures, Phys. Rev. B **100**, 134501 (2019).

[20] T. T. Heikkila, R. Ojajarvi, I. J. Maasilta, E. Strambini, F. Giazotto and F. S. Bergeret, Thermoelectric Radiation Detector Based on Superconductor-Ferromagnet Systems, Phys. Rev. Applied **10**, 034053 (2018).

[21] J. A. Ouassou, C. González-Ruano, D. Caso, F. G. Aliev, and J. Linder, Complete magnetic control over the superconducting thermoelectric effect, Phys. Rev. B **106**, 094514 (2022).

[22] I. Martínez, C. Tiusan, M. Hehn, M. Chshiev and F. G. Aliev, Symmetry broken spin reorientation transition in epitaxial MgO/Fe/MgO layers with competing anisotropies, Sci Rep **8**, 9463 (2018).

[23] M. S. Gabor, T. Petrisor, Jr., C. Tiusan, M. Hehn, and T. Petrisor, Magnetic and structural anisotropies of Co_2FeAl Heusler alloy epitaxial thin films, Phys. Rev. B **84**, 134413 (20211).

[24] K.D. Usadel, Generalized diffusion equation for superconducting alloys. Phys. Rev. Lett. **25**, 507 (1970).

[25] J. Rammer and H. Smith, Quantum field-theoretical methods in transport theory of metals. Rev. Mod. Phys. **58**, 323.

[26] F.S. Bergeret, M. Silaev, P. Virtanen, T.T. Heikkilä, Colloquium: Nonequilibrium effects in superconductors with a spin-splitting field. Rev. Mod. Phys. **90**, 041001 (2018).

[27] V. Chandrasekhar, Superconductivity, edited by K. Bennemann and J. Ketterson (Springer, Berlin, 2008).

[28] W. Belzig, F.K. Wilhelm, C. Bruder, G. Schön, A.D. Zaikin, Quasiclassical Green's function approach to mesoscopic superconductivity. Superlattices and Microstructures **25**, 1251 (1999).

[29] J.A. Ouassou, A. Pal, M. Blamire, M. Eschrig, J. Linder, Triplet Cooper pairs induced in diffusive s-wave superconductors interfaced with strongly spin-polarized magnetic insulators or half-metallic ferromagnets. Sci Rep **7**, 1932 (2017).

[30] M. Eschrig, A. Cottet, W. Belzig, J. Linder, General boundary conditions for quasiclassical theory of superconductivity in the diffusive limit: application to strongly spin-polarized systems. New J. Phys. **17**, 083037 (2015).

[31] A. Cottet, D. Huertas-Hernando, W. Belzig, Y.V. Nazarov, Spin-dependent boundary conditions for isotropic superconducting Green's functions. Phys. Rev. B **80**, 184511 (2009).

[32] A. Cottet, Spectroscopy and critical temperature of diffusive superconducting/ferromagnetic hybrid structures with spin-active interfaces. Phys. Rev. B **76**, 224505 (2007).

[33] S.H. Jacobsen, J.A. Ouassou, J. Linder, Critical temperature and tunneling spectroscopy of superconductor-ferromagnet hybrids with intrinsic Rashba-Dresselhaus spin-orbit coupling. Phys. Rev. B **92**, 024510 (2015).

[34] N. Schopohl, Transformation of the Eilenberger equations of superconductivity to a scalar Riccati equation. Unpublished.

[35] J.A. Ouassou, T.D. Vethaak, J. Linder, Voltage-induced thin-film superconductivity in high magnetic fields. Phys. Rev. B **98**, 144509 (2018).

[36] C. Rau, C. Liu, A. Schmalzbauer, and G. Xing, Ferromagnetic Order at (100) $p(1 \times 1)$ Surfaces of Bulk Paramagnetic Vanadium, Phys. Rev. Lett. **57**, 2311 (1986).

[37] D. R. Grempel and S. C. Ying, Spin Fluctuations at the Surface of Vanadium, Phys. Rev. Lett. **45**, 1018 (1980).

[38] T. G. Walker and H. Hopster, Induced magnetic order in ultrathin vanadium films on Fe(100), Phys. Rev. B **49**, 7687 (1994).

[39] P. Fuchs, K. Totland, and M. Landolt, Induced magnetization in thin epitaxial V films on Fe (100), Phys. Rev. B **53**, 9123 (1996).

[40] T. Bryk, D. M. Bylander, and L. Kleinman, Magnetism of the V(001) surface in the generalized gradient approximation, Phys. Rev. B **61**, R3780(R) (2000).

[41] D. Lacina, J. Yang, and J. L. Erskine, Multilayer relaxation and search for ferromagnetic order at the (100) surface of bulk paramagnetic vanadium, Phys. Rev. B. **75**, 195423 (2007).

[42] A. Rubio-Ponce, D. Olguín, A. Aguayo and R. de Coss, Surface magnetism in vanadium overlayers on W(100), Journal of Magnetism and Magnetic Materials **514**, 15, 167143 (2020).

[43] C. Tiusan, M. Hehn, F. Montaigne, F. Greullet, S. Andrieu and A. Schuhl, Spin tunneling phenomena in single crystal magnetic tunnel junction systems, J. Phys.: Condens. Matter **19**, 165201 (2007).

[44] C. González-Ruano, D. Caso, L. G. Johnsen, C. Tiusan, M. Hehn, N. Banerjee, J. Linder and Farkhad G. Aliev, Superconductivity assisted change of the perpendicular magnetic anisotropy in V/MgO/Fe junctions, Scientific Reports **11**, 19041 (2021).

[45] COMSOL Multiphysics® www.comsol.com. COMSOL AB, Stockholm, Sweden.

[46] M. Dixon, F. E. Hoare, T. M. Holden and D. E. Moody, The Low Temperature Specific Heats of Some Pure Metals (Cu, Ag, Pt, Al, Ni Fe Co), Proceedings of the Royal Society of London. Series A, Mathematical and Physical Sciences **285**, 1403, 561-580 (1965).

[47] J.W. Gardner and A. C. Anderson, Effect of neutron irradiation on the low-temperature specific heat and thermal conductivity of magnesium oxide, Phys. Rev. B **23** 415 (1981).

[48] Jung, Wayne Douglas, The thermal conductivity of high purity vanadium, Retrospective Theses and Dissertations. Paper 5485 (1975).

[49] R. Radebaugh and P. H. Keesom, Low-Temperature Thermodynamic Properties of Vanadium. Phys. Rev. **149**, 19 (1966).

[50] M. Walter, J. Walowski, V. Zbarsky, M. Munzenberg, M. Schafers,

D. Ebke, G. Reiss, A. Thomas, P. Peretzki, M. Seibt, J. S. Moodera, M. Czerner, M. Bachmann and C. Heiliger, Seebeck effect in magnetic tunnel junctions, Nature Materials **10**, 742–746 (2011).